Available online at www.sciencedirect.com
ScienceDirect
Applied Catalysis B: Environmental 82 (2008) 190–198
APPLIED CATALYSIS B: ENVIRONMENTAL
www.elsevier.com/locate/apcatb

New sulfur adsorbents derived from layered double hydroxides I: Synthesis and COS adsorption

Dennis E. Sparks, Tonya Morgan, Patricia M. Patterson, S. Adam Tackett, Erin Morris, Mark Crocker *

Center for Applied Energy Research, University of Kentucky, 2540 Research Park Drive, Lexington, KY 40511-8479, USA

Received 21 August 2007; received in revised form 21 December 2007; accepted 15 January 2008
Available online 20 January 2008

Abstract

Mixed oxides, prepared via the thermal decomposition of layered double hydroxides (LDHs), were screened gravimetrically for their ability to adsorb carbonyl sulfide (COS). Based on promising results obtained for Ni/Mg/Al, Ni/Mg/Fe and Co/Mg/Al mixed oxides, a study was undertaken to optimize the composition of these materials for COS adsorption. To investigate the effect of the M(II):M(III) ratio, LDHs of the type $[M_zMg_yAl_x(OH)_2](CO_3)_{x/2}{\cdot}0.5H_2O$ (where M = Ni or Co, and $x + y + z = 1$) were prepared at values of x corresponding to 0.33 and 0.20. Simultaneously, the elemental ratio of transition metal to magnesium (z/y) was varied. Mixed oxides obtained from the resulting LDHs were tested in fixed bed mode with a feed of 100 ppm COS in N_2 to determine breakthrough capacity. In general Ni/Mg/Al mixed oxides showed the best performance, a composition with Ni/Mg/Al = 0.32/0.48/0.20 showing the best adsorption capacity. Treatment of the spent adsorbent under an atmosphere of 5% H_2 in N_2 at 450 °C was found to provide an effective means of restoring the adsorption capacity over two cycles of adsorption and regeneration, although after three such cycles, adsorption capacity decreased.

Keywords: Adsorption; Carbonyl sulfide; Methyl mercaptan; Layered double hydroxide; Hydrotalcite

1. Introduction

In order for hydrocarbon fuels or coal-derived syngas to be used as feedstocks for fuel cells, their sulfur content must be reduced to very low levels. Sulfur is particularly problematic for Proton Exchange Membrane Fuel Cells (PEMFCs); at their low operating temperature (~80 °C), sulfur compounds adsorb strongly on the Pt electrocatalyst, blocking surface sites for hydrogen adsorption and dissociation. Uribe and Zawodzinski [1] have reported that H_2S concentrations as low as 0.2 parts per million by volume (ppmv) adversely affect the performance of PEMFCs, a finding which has recently been confirmed by de Bruijn and co-workers [2]. Further, sulfur compounds are poisons for any base metal catalysts used in the fuel processor. Consequently, in order to maximize durability it is necessary to set the allowable sulfur concentration at levels as low as <10 ppb [3].

The form and concentration of sulfur compounds present varies significantly between feedstocks. Natural gas and liquified petroleum gas (LPG) constitute two feedstocks particularly suited for residential and commercial PEMFC applications as a result of the highly developed infrastructure that exists for their distribution. The sulfur content of pipeline natural gas in the USA is typically between 4 and 8 ppmw, corresponding to H_2S, carbonyl sulfide (COS), methyl mercaptan and trace amounts of dimethylsulfide [4]. In addition, a maximum of 12 ppmw of odorants is permitted. Tertiary butyl mercaptan (*t*-BuSH) is the most commonly used odorant and is frequently blended with other mercaptans such as *i*-PrSH (in order to depress the freezing point), as well as sulfides such as Me_2S and MeSEt (added for their resistance to oxidation and high soil penetrability) [5]. Commercial-grade liquified petroleum gas has a maximum allowable sulfur content of 185 ppmw, while that for HD-5 grade LPG, designed for use in internal combustion engines, is 123 ppmw [6]. EtSH is the most widely used odorant for LPG [5], added at levels up to 30 ppm.

Direct removal of sulfur contaminants via adsorption is a particularly attractive means of achieving the low sulfur levels

* Corresponding author. Tel.: +1 859 257 0295; fax: +1 859 257 0302.
E-mail address: crocker@caer.uky.edu (M. Crocker).

0926-3373/$ – see front matter © 2008 Elsevier B.V. All rights reserved.
doi:10.1016/j.apcatb.2008.01.012

required for fuel cell feedstocks. For consumer systems, the adsorbent(s) could be contained in a cartridge which is replaced at specific intervals, i.e., when the adsorbent is approaching saturation. Alternative approaches to sulfur removal include hydrotreating or thermal cracking of the organosulfur contaminants, followed by adsorption of the H_2S product on zinc oxide, both processes typically operating at temperatures in the range 280–400 °C [7,8]. Among the various sulfur contaminants present, the removal of COS is particularly problematic as thermodynamic constraints dictate that only partial conversion of COS is possible via hydrotreating [8]:

$$\mathrm{COS} + \mathrm{H_2} \rightleftarrows \mathrm{CO} + \mathrm{H_2S} \qquad K = \frac{[\mathrm{H_2S}][\mathrm{CO}]}{[\mathrm{COS}][\mathrm{H_2}]} = 10.9 \text{ at } 327\,^{\circ}\mathrm{C}$$

Commercially, COS is removed either by adsorption or via catalytic hydrolysis at temperatures around 200 °C or higher, followed by adsorption of the H_2S product:

$$\mathrm{COS} + \mathrm{H_2O} \rightleftarrows \mathrm{CO_2} + \mathrm{H_2S}$$

$$K = \frac{[\mathrm{H_2S}][\mathrm{CO_2}]}{[\mathrm{COS}][\mathrm{H_2O}]} = 2.75 \times 10^3 \text{ at } 200\,^{\circ}\mathrm{C}$$

The latter method possesses the advantage that H_2S can be readily removed using a variety of inexpensive adsorbents such as ZnO. In contrast, COS, being less acidic and less polar than H_2S, is harder to remove using conventional adsorbents.

To date, a number of different types of adsorbent have been described in the patent and open literature for the desulfurization of hydrocarbon streams. These include supported metal oxides (where the support is typically alumina or carbon), mixed metal oxides, metal ion-exchanged zeolites and activated carbons. While a number of materials are claimed in patents to be effective for the removal of COS, in general elevated operating temperatures are required [9,10].

In this work we describe the synthesis of a series of mixed metal oxides derived from double layered hydroxides which show promise as ambient temperature COS adsorbents. Layered double hydroxides (LDHs), also referred to as hydrotalcite-like compounds, comprise a class of compounds that are increasingly receiving attention because of their properties as ion exchangers, adsorbents, catalysts and catalyst supports [11–15]. LDHs have the general formula $[M(II)_{1-x}\text{-}M(III)_x(OH)_2]^{x+}(A_{x/n}{}^{n-})\cdot mH_2O$. The structure consists of positively charged brucite-like ($Mg(OH)_2$) layers with the trivalent cations substituting for divalent cations in the octahedral sites of the sheets. Upon heating the clay structure collapses and mixed metal oxides are formed. The latter are of particular interest due to their high surface area, homogeneous mixing of the different elements and increased basicity relative to the precursor LDHs [11], rendering them prime candidates for adsorbent applications. Indeed, calcined LDHs have been shown to be effective adsorbents for acidic species such as CO_2 [16–18], NO_x [19,20], and SO_x [15,21–23]. The use of calcined LDHs for the removal of mercaptans, organosulfides, H_2S, CS_2 and thiophene from hydrocarbon streams has also been claimed [24].

Given that the surface properties of LDHs and the mixed oxides derived from them depend strongly on their chemical composition, we have examined a series of LDH-derived mixed metal oxides containing differing ratios of Mg to Al. In addition, mixed metal oxides were prepared in which some, or all, of the Mg ions were replaced by other divalent transition metal ions. The adsorption capacities of the resulting materials for COS and CH_3SH have been assessed.

2. Experimental

2.1. Adsorbent preparation

Unless otherwise stated, layered double hydroxides were prepared by precipitation under conditions of low supersaturation. Two solutions, one containing the appropriate metal nitrates and one containing a mixture of NaOH and Na_2CO_3, were simultaneously added and mixed while maintaining a constant pH (usually 8–10) [11]. In addition, selected Mg/Al LDHs were prepared by means of precipitation at high supersaturation, in which the metal nitrates solution was added to the base solution at high pH [25]. In both cases the concentration of the metal nitrate solution used was 1.5 M (total metals), while the base solution contained Na_2CO_3 (1.0 M) and the calculated amount of NaOH (~3 M) required for complete reaction with the divalent and trivalent metal ions. The solutions were mixed at room temperature at an addition rate of ~3 ml min^{-1}, with vigorous mechanical stirring. Unless otherwise stated, the precipitate was aged in the synthesis solution overnight at 70 °C and isolated by a cycle of centrifuging/decanting/washing with deionized water until the washings attained a pH of 7. The resulting solid was dried at 60 °C in a vacuum oven. The measured residual sodium content was in all cases <500 ppm. In addition, a commercial Mg/Al LDH (MG70) was obtained from Sasol. To produce mixed oxides, the LDHs were calcined in air at 450 °C for 2 h.

High surface area MgO was prepared by a standard precipitation method [26]. Samples of commercial adsorbents were provided by Air Products and comprised Calgon type FCA carbon (CuO/Cr_2O_3 impregnated onto activated carbon), Calgon Sulfusorb 12 (CuO impregnated onto activated carbon), and Air Products AgLiX zeolite.

2.2. Adsorbent characterization

Elemental analyses were performed using XRF. In general, good agreement was found between the measured and nominal LDH compositions, i.e., the measured metal ion ratios were the same as those used in the synthesis solution within analytical error. Surface area measurements on the LDHs, before and after calcination, were performed using a Micromeritics Tristar 3000 gas adsorption analyzer, using the BET method from nitrogen adsorption isotherms at 77 K. The samples were outgassed at 160 °C overnight prior to analysis. Powder X-ray diffraction (XRD) measurements were performed on a Phillips X'Pert diffractomer using Cu Kα radiation (λ = 1.5406 Å) and a step size of 0.02°. Peak simulation was performed using a standard

fitting program [27]. Average crystallite sizes were calculated using Fourier integral breadth analysis. Calculations were based on the (0 0 3) line at *ca.* $2\theta = 12^{\circ}$, this being the most intense line in the XRD patterns. Weight loss on thermal treatment was determined using a Seiko Instruments Inc. TG/DTA 320 simultaneous thermogravimetric/differential thermal analyzer coupled to a Micromass PC residual gas analyzer system. The samples were heated in a flow of inert gas at 10 °C min^{-1} from room temperature to 700 °C.

2.3. Gravimetric adsorption studies

Gravimetric adsorption tests were performed on powder samples using a Thermal Analysis TGA system. In each case the LDH was initially activated by heating at 10 °C min^{-1} in 100 cm^3 min^{-1} N_2 to 450 °C and holding at 450 °C for 75 min to generate the mixed oxide. The sample was then allowed to cool to room temperature in flowing N_2. Carbonyl sulfide (300 ppm in N_2) or methyl mercaptan (CH_3SH, 300 ppm in N_2), was flowed over the sample for 1000 min and the gain in sample weight was monitored.

2.4. Fixed bed adsorption studies

Fixed bed adsorption studies were performed at 20 °C and atmospheric pressure in a tubular stainless steel reactor, using 0.5 g of material (0.55–0.93 mm sieve fraction). Prior to each adsorption run, the LDH was calcined in air in a muffle furnace (450 °C, 2 h), during which the sample lost *ca.* 35% of its initial weight. A weighed amount of the material was then transferred to the reactor and further treated at 450 °C in flowing He for 1 h. In the case of commercial adsorbents, the sample was dried *in situ* by heating at 200 °C in He for 1 h. The dimensions of the adsorbent bed were typically 40 mm × 7 mm (l/*d* of *ca.* 6), the adsorbent being held in place by plugs of glass wool. The feed consisted of either 100 ppm COS in N_2 or 100 ppm CH_3SH in N_2. A flow rate of 15 cm^3 min^{-1} was used, equivalent to a gas hourly space velocity (GHSV) of *ca.* 1800 h^{-1}. Gas analyses were carried out using Sensidyne detector tubes for COS (tube no. 239S) and CH_3SH (tube no. 164SA). The specified detection limits are 2 ppm and 1 ppm, respectively, for a 100 ml gas sample. In principle, by flowing larger gas samples through the detector tubes, correspondingly lower detection limits can be achieved (e.g., 0.2 and 0.1 ppm, respectively, for a 1000 ml sample). The estimated detection level for the gas sample sizes typically used in this study was 0.5 ppm for both COS and CH_3SH. Breakthrough times were determined graphically, by extrapolating the COS measurements after breakthrough back to the initial breakthrough point.

Adsorbent regeneration was performed *in situ*. At the end of the adsorption run the feed gas was switched to 5% H_2 in N_2 (36 cm^3 min^{-1}) and the sample heated to 450 °C (10 °C min^{-1}). After holding for 1 h at this temperature the gas flow was switched to He and the sample allowed to cool to room temperature overnight, after which a new adsorption run was commenced. In cases where samples of the regenerated adsorbent were taken for analysis, the adsorbent was first passivated in a flow of 1% O_2 in He.

3. Results and discussion

3.1. Characterization of adsorbents for screening studies

The chemical composition and corresponding physical data for the LDHs used for the initial gravimetric screening studies are given in Table 1. All of the samples exhibited X-ray

Table 1
Chemical composition and physical characterization of LDH-derived adsorbents used for gravimetric adsorption experiments

Sample composition (atomic ratio)	Synthesis pH	Surface area of LDH (m^2 g^{-1})	Crystallite size (LDH) (Å)[e]	Surface area of mixed oxide (m^2 g^{-1})
Mg/Al = 0.65/0.35	∼13[a]	74	204	136
Mg/Al = 0.73/0.27	∼13[a]	80	169	209
Mg/Al = 0.49/0.51	10[b]	155	59	253
Mg/Al = 0.74/0.26	10[c]	107	107	267
Mg/Al = 0.74/0.26	–[d]	19	178	182
Cu/Mg/Al = 0.33/0.33/0.34	8	74	135	93
Zn/Mg/Al = 0.37/0.31/0.32	8	103	69	136
Co/Mg/Al = 0.34/0.29/0.37	10	167	47	196
Ni/Mg/Al = 0.33/0.33/0.34	10	196	46	258
Cu/Zn/Al = 0.37/0.44/0.19	8	37	167	72
Ni/Mg/Fe = 0.32/0.32/0.36	10	152	81	159
Co/Mg/Fe = 0.35/0.29/0.36	10	85	101	106
Co/Ni/Al = 0.37/0.39/0.24	10	131	74	128
Co/Ni/Al = 0.41/0.28/0.31	10	53	228	62
Zn/Al = 0.77/0.23	8	98	77	114
Co/Fe = 0.75/0.25	7	52	250	78
MgO	–	–	–	205

[a] High supersaturation method; pH quoted corresponds to final value.
[b] Aging for 1 h at 20 °C.
[c] Aging for 20 h at 20 °C.
[d] Commercially available LDH.
[e] Determined in 0 0 *l* direction.

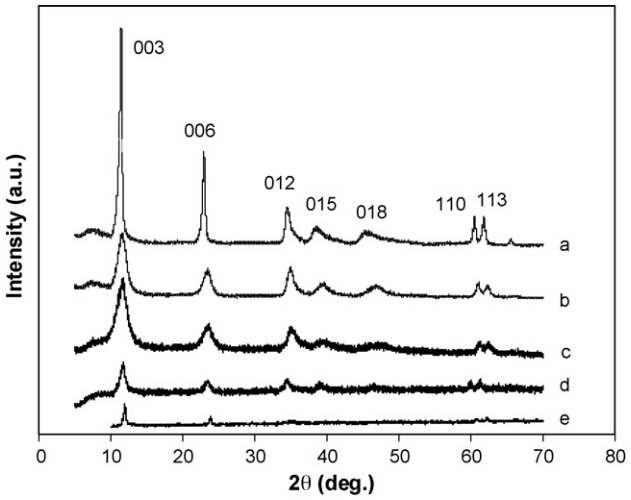

Fig. 1. X-ray diffractograms of selected LDHs: (a) Mg/Al = 0.74/0.26, (b) Mg/Al = 0.49/0.51, (c) Ni/Mg/Al = 0.33/0.33/0.34, (d) Ni/Mg/Fe = 0.32/0.32/0.36, and (e) Co/Ni/Al = 0.41/0.28/0.31.

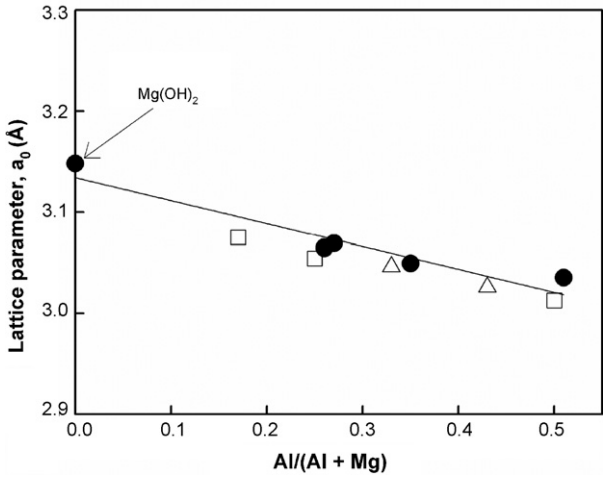

Fig. 2. Lattice parameter, a_0, as a function of Al^{3+} content for Mg/Al LDHs. (●) This work; (△) Tsuji et al. [28] and (□) Di Cosimo et al. [29].

diffractograms characteristic of hydrotalcite-type compounds (see Fig. 1), with symmetric reflections for (0 0 3), (0 0 6), (1 1 0) and (1 1 3) planes, and broader, asymmetric peaks for (0 1 2), (0 1 5) and (0 1 8) planes. Significant differences were observed with respect to the crystallinity of the samples, the strongest X-ray reflections being observed for the Mg/Al LDHs aged at 70 °C. The lattice parameter, a_0, is known to decrease with an increase in Al^{3+} substitution in the brucite-like layer because the ionic radius of Al^{3+} (0.535 Å) is smaller than that of Mg^{2+} (0.720 Å) [28]. The unit cell parameter, a_0, was calculated for all the Mg/Al LDHs, based on hexagonal symmetry, and the results are presented in Fig. 2 as a function of the Al/(Al + Mg) ratio. There is good agreement with values reported in the literature [28,29], the observed lattice expansion being consistent with the presence of a single LDH phase in all cases.

The crystallite sizes of the LDHs, as calculated from their diffractograms, are listed in Table 1. Crystallite sizes calculated for a number of the ternary samples indicate a tendency towards less ordered structures in comparison with the Mg/Al LDHs. Diffractogram (c) in Fig. 1 shows the line broadening in evidence for the Ni/Mg/Al sample.

For the Mg–Al LDHs, those aged at 20 °C have surface areas in excess of 100 $m^2\ g^{-1}$, in contrast to the samples aged at 70 °C. Previous studies have shown that increasing the severity of Mg/Al LDH aging results in increased crystallinity (and

Table 2
Summary of COS and CH_3SH gravimetric adsorption experiments

Sample composition[a]	Weight gain COS (%) after 1000 min	Normalized COS uptake (μmol m^{-2})	Weight gain CH_3SH (%) after 1000 min	Normalized CH_3SH uptake (μmol m^{-2})
Mg/Al = 0.65/0.35	2.7	3.3	2.2	3.4
Mg/Al = 0.73/0.27	3.5	2.8	2.6	2.6
Mg/Al = 0.49/0.51	3.9	2.6	3.1	2.5
Mg/Al = 0.74/0.26	3.4	2.1	–	–
Mg/Al = 0.74/0.26[b]	3.4	3.1	3.6	4.1
Cu/Mg/Al = 0.33/0.33/0.34	3.2	5.7	–	–
Zn/Mg/Al = 0.37/0.31/0.32	3.9	4.8	–	–
Co/Mg/Al = 0.34/0.29/0.37	5.5	4.7	5.5	5.8
Ni/Mg/Al = 0.33/0.33/0.34	5.6	3.6	4.8	3.9
Cu/Zn/Al = 0.37/0.44/0.19	1.8	4.2	–	–
Ni/Mg/Fe = 0.32/0.32/0.36	6.2	6.5	–	–
Co/Mg/Fe = 0.35/0.29/0.36	3.2	5.0	–	–
Co/Ni/Al = 0.37/0.39/0.24	5.0	6.5	–	–
Co/Ni/Al = 0.41/0.28/0.31	5.5	14.8	–	–
Zn/Al = 0.77/0.23	1.7	2.5	–	–
Co/Fe = 0.75/0.25	2.3	4.9	–	–
MgO	4.8	3.9	–	–
Calgon Sulfusorb 12	1.5	–	4.8	–
Calgon FCA	4.3	–	–	–
Air Products AgLiX	7.3	–	6.0	–

[a] Physical characterization data given in Table 1.
[b] Mixed oxide derived from commercially available LDH.

hence larger crystallite sizes), with a corresponding decrease in surface area [30]. Additional factors known to influence the surface area include the nature of the metal ions incorporated and the preparation route [11]. In the case of the ternary LDHs there is no obvious systematic dependency of the BET surface area on the transition metal ion, although in agreement with a previous report, the Co/Mg/Al LDH has a greater surface area than the Cu/Mg/Al LDH [15].

Calcination at 450 °C resulted in decomposition of the LDHs into the corresponding mixed oxides, with an accompanying increase in BET surface area (Table 1). It was not possible to determine any structural parameters from the X-ray diffactograms for the mixed oxides (not shown) as they were much less ordered structures. Thermogravimetric analyses of the LDHs were performed, the weight loss profiles being characterized by two distinct weight loss regions [11]. The first, corresponding to a dTG maximum of *ca.* 230 °C, is associated with the release of water in the interlayer. The second weight loss occurs at higher temperature (∼425 °C) and represents the simultaneous loss of CO_2 from the interlayer region and dehydroxylation of the LDH sheets, resulting in the collapse of the clay structure. All of the LDHs prepared exhibited this characteristic weight loss profile.

3.2. Gravimetric adsorption studies

Gravimetric adsorption experiments were performed as a means of rapidly screening the LDH-derived mixed oxides for COS adsorption capacity. Table 2 presents the results of the experiments, which were performed at ambient temperature and pressure. Given that diffusional limitations in the TGA instrument are expected to be significant, the measured adsorption capacities are taken to be indicative of relative, rather than absolute, adsorption capacities. The adsorption is quoted as a weight gain after 1000 min on stream and represents the uptake on the mixed oxides after thermal activation at 450 °C, this having been found to be the optimal activation temperature based on exploratory experiments. Fig. 3 shows the adsorption profiles for selected mixed oxides. Consideration of the Mg–Al materials reveals no apparent trend between the Al content and COS uptake. This contrasts with the results of a study by Di Cosimo et al. [29] of CO_2 adsorption on Mg–Al mixed oxides derived from the thermal decomposition of LDHs at 400 °C. CO_2 adsorption capacity, normalized on the basis of surface area, was found to follow the sequence $0 > 0.11 > 0.47 > 0.65 > 0.24 > 0.18 > 1.0$ with respect to the Al/(Mg + Al) ratio. These results were explained on the basis that at low Al/(Mg + Al) ratios (<0.2) the basic site density is decreased relative to MgO, due to the presence of a surface AlO_x phase which partially covers the main MgO phase, thereby decreasing the surface concentration of O^{2-} anions. At higher ratios ($0.2 < Al/(Mg + Al) < 0.5$), a mixed Mg–Al oxide phase is formed, causing the number of defects to increase and the partial recovery of the basic site density. In samples with Al/(Mg + Al) > 0.5, demixing of the Mg–Al phase occurs, leading to bulk $MgAl_2O_4$ spinels and a decrease in basic site density. In the present work, measured COS uptake values for the Mg–Al mixed oxides fell in a rather narrow range of 2.1–3.3 μmol m^{-2} (Table 2), with no obvious dependence on the Al/(Mg + Al) ratio. Hence COS uptake measured on a weight basis is dependent to a large degree on the surface area of the samples. However, in keeping with the findings of Di Cosimo et al. for CO_2 adsorption [29], MgO was found to display the greatest normalized COS uptake, corresponding to a value of 3.9 μmol m^{-2}.

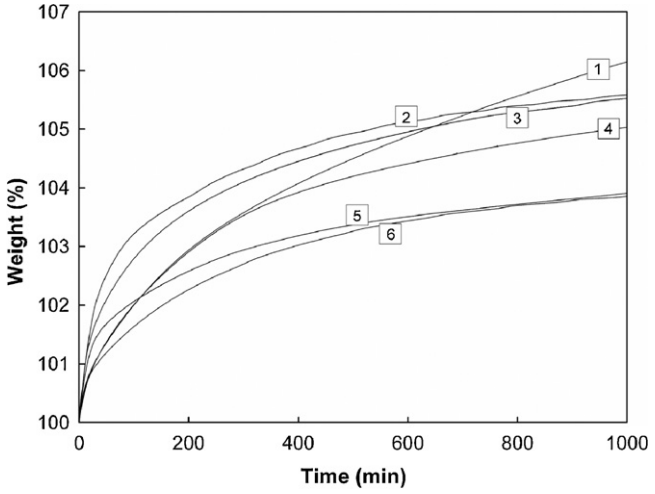

Fig. 3. Gravimetric adsorption profiles for COS on mixed oxides generated by thermal decomposition of LDHs: (1) Ni/Mg/Fe = 0.33/0.33/0.36; (2) Ni/Mg/Al = 0.33/0.33/0.34; (3) Co/Mg/Al = 0.34/0.29/0.37; (4) Co/Ni/Al = 0.37/0.39/0.24; (5) Mg/Al = 0.49/0.51; (6) Zn/Mg/Al = 0.37/0.31/0.32.

As shown in Table 2, substituting some of the Mg by Co, Ni, Cu or Zn ions was found to increase the normalized COS uptake. The exception to this was the Zn–Al mixed oxide, the low COS uptake displayed by this material presumably being related to its low basicity. Given the rather low surface areas of the ternary mixed oxide compositions containing Cu and Zn, these materials do not represent an improvement on Mg/Al mixed oxides when COS uptake is measured on a weight basis. Conversely, the ternary oxides containing Ni and Co display the highest COS uptake on a weight basis, due in part to their moderate to high surface areas. These findings are broadly consistent with the literature concerning CO_2 adsorption [28]: for binary LDHs activated at temperatures in the range 200–400 °C, Mg/Al (and also Ni/Al and Co/Al) materials are found to possess significantly higher adsorption capacities on a weight basis than the Zn/Al and Cu/Al analogues.

The effect of replacing Al with Fe in the ternary oxides was also studied. For the Co/Mg/Fe mixed oxide this resulted in almost no change in the normalized COS uptake, while its low surface area resulted in a lower uptake on a weight basis. In contrast, comparison of the results for Ni/Mg/Fe and Ni/Mg/Al materials reveals higher COS uptake for the Ni/Mg/Fe oxide on both a normalized and a weight basis. In addition to the LDH-derived mixed oxides, three commercial adsorbents were tested for comparative purposes. As can be seen from Table 2, several of the ternary mixed oxides studied, e.g., Ni/Mg/Fe, Ni/Mg/Al and Co/Mg/Al, compare very favorably with the commercial carbon-based adsorbents, albeit that they show lower COS

Table 3
Chemical composition and physical characterization of LDH-derived adsorbents used for fixed bed adsorption experiments

Sample composition (atomic ratio)[a]	Surface area of LDH ($m^2\ g^{-1}$)	Crystallite size (LDH) (Å)[b]	Surface area of mixed oxide ($m^2\ g^{-1}$)
Mg/Al = 0.75/0.25	139	64	242
Ni/Al = 0.67/0.33	162	73	180
Ni/Mg/Al = 0.54/0.13/0.33	180	47	207
Ni/Mg/Al = 0.40/0.27/0.33	179	49	281
Ni/Mg/Al = 0.27/0.40/0.33	175	52	255
Ni/Mg/Al = 0.13/0.54/0.33	159	67	276
Ni/Al = 0.80/0.20	167	38	197
Ni/Mg/Al = 0.64/0.16/0.20	156	44	219
Ni/Mg/Al = 0.48/0.32/0.20	148	44	253
Ni/Mg/Al = 0.32/0.48/0.20	64	49	252
Ni/Mg/Al = 0.16/0.64/0.20	89	55	224
Co/Mg/Al = 0.54/0.13/0.33	45	43	119
Co/Mg/Al = 0.13/0.54/0.33	61	180	156
Co/Mg/Al = 0.64/0.16/0.20	32	68	96
Co/Mg/Al = 0.16/0.64/0.20	77	85	242

[a] Nominal ratios: Values determined by XRF were found to agree to within ±10%. All samples prepared by precipitation at pH 10.
[b] Determined in 0 0 *l* direction.

uptake than the AgLiX zeolite. Data for methyl mercaptan (CH_3SH) adsorption are also given in Table 2; these appear to follow a similar trend to COS adsorption.

3.3. Adsorbent optimization

Given the promising results obtained above for the Ni/Mg/Al, Ni/Mg/Fe and Co/Mg/Al mixed oxides, an effort was made to optimize the composition of these materials for COS adsorption. To investigate the effect of the M(II):M(III) ratio, LDHs of the type $[M_zMg_yAl_x(OH)_2](CO_3)_{x/2}{\cdot}0.5H_2O$ (where M = Ni or Co, and $x + y + z = 1$) were prepared at values of x corresponding to 0.33 and 0.20. Simultaneously, the elemental ratio of transition metal to magnesium (z/y) was varied. The physical properties of the resulting materials are collected in Table 3. The phase purity of the resulting LDHs was checked using powder X-ray diffraction and found to be satisfactory in all cases, i.e., no extraneous phases were detected. Comparison of the measured BET surface areas of the LDHs reveals several trends. First, for the Ni/Mg/Al LDHs, surface areas of the materials with $x = 0.33$ are slightly higher than those with $x = 0.20$, i.e., high Al content tends to favor high surface areas. This can be attributed to the fact that higher layer charge results in the expulsion of increased amounts of CO_2 and H_2O during calcination, and hence increased generation of new pores. Second, within the two series of Ni/Mg/Al LDHs, there is a tendency for surface area to increase with increasing Ni/Mg ratio. Third, surface areas of the Ni/Mg/Al LDHs are considerably higher than those of their Co analogs. The high surface areas of the Ni/Mg/Al LDHs are reflected in small crystallite sizes, with consequent broadening of their XRD diffraction peaks (Fig. 4). In all cases, calcination resulted in the formation of mixed oxides possessing increased surface area relative to the LDH. For the Ni/Mg/Al materials there was no correlation between the surface area of the LDH and corresponding mixed oxide, although as for the LDHs, the Ni/Mg/Al mixed oxides possessed higher surface areas than their Co/Mg/Al analogs.

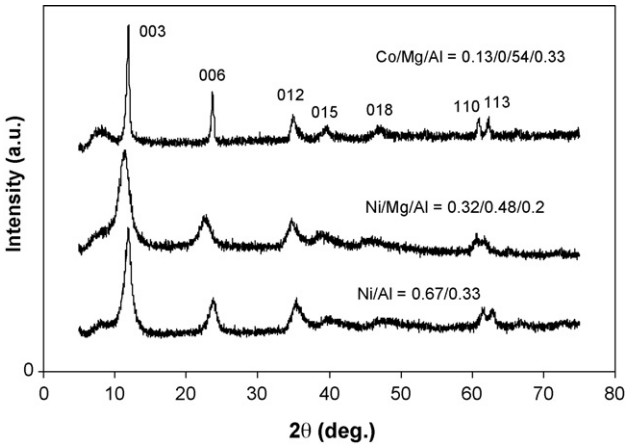

Fig. 4. X-ray diffractograms of selected LDHs used for fixed bed adsorption experiments.

3.4. Carbonyl sulfide adsorption

In order to determine the breakthrough capacities of the mixed oxides, fixed bed COS adsorption experiments were performed. The results of the various runs, conducted at 20 °C, are collected in Table 4. For all the adsorbents tested, the measured COS concentration at the bed outlet remained below the detection limit (~0.5 ppm) up to the point of breakthrough (Fig. 5). Consideration of the breakthrough capacities reveals several trends:

- Ni/Mg/Al adsorbents are superior to their Co/Mg/Al analogs, however, this appears to be largely due to the higher surface areas of the former: on a normalized basis, the COS adsorption capacities are similar.
- Replacing Al with Fe has a deleterious effect on adsorption capacity (on both an absolute and normalized basis), as reflected in results obtained for the Ni/Mg/(Al or Fe) = 0.33/0.33/0.33 mixed oxides.
- For the two series of Ni/Mg/Al materials with different Al contents, the materials with the lower Al content ($x = 0.20$) have higher adsorption capacities than their high Al content analogs ($x = 0.33$). This effect is not associated with the surface areas of the mixed oxides (as reflected in the normalized uptake values) and implies that the COS adsorption sites in these materials are associated with Ni^{2+} and Mg^{2+}, rather than with Al^{3+}. Consideration of the data for the Co/Mg/Al mixed oxides similarly suggests that COS adsorption on these materials is associated primarily with the Co and Mg ions.

On the other hand, no relationship could be found between COS adsorption capacity and the Ni/Mg ratio. Neither of the two series of Ni/Mg/Al materials shows any correlation in this

Table 4
Summary of COS and CH_3SH fixed bed adsorption experiments

Sample	Co	Ni	Mg	Al	Fe	Wt% COS captured	Normalized COS uptake (μmol m^{-2})	Wt% CH_3SH captured	Normalized CH_3SH uptake (μmol m^{-2})
Mg/Al			0.73	0.27		0.93	1.95	–	–
Mg/Al			0.75	0.25		1.37	0.94	–	–
Co/Mg/Al	0.33		0.33	0.33		0.89	0.89	–	–
Ni/Mg/Al		0.33	0.33	0.33		1.61	1.37	–	–
Ni/Mg/Fe		0.33	0.33		0.33	0.88	0.96	–	–
Ni/Al		0.67		0.33		0.77	0.71	–	–
Ni/Mg/Al		0.54	0.13	0.33		1.37	1.10	–	–
Ni/Mg/Al		0.40	0.27	0.33		0.87	0.52	–	–
Ni/Mg/Al		0.27	0.40	0.33		0.83	0.54	–	–
Ni/Mg/Al		0.13	0.54	0.33		1.29	0.78	–	–
Ni/Al		0.80		0.20		1.49	1.26	–	–
Ni/Mg/Al		0.64	0.16	0.20		1.80	1.37	2.42	2.30
Ni/Mg/Al		0.48	0.32	0.20		1.56	1.03	–	–
Ni/Mg/Al		0.32	0.48	0.20		2.47	1.64	3.47	2.87
Ni/Mg/Al		0.16	0.64	0.20		1.77	1.32	–	–
Co/Mg/Al	0.54		0.13	0.33		0.83	1.16	–	–
Co/Mg/Al	0.13		0.54	0.33		1.06	1.13	–	–
Co/Mg/Al	0.64		0.16	0.20		1.03	1.79	–	–
Co/Mg/Al	0.16		0.64	0.20		1.00	0.69	–	–
Air Products AgLiX						3.52	–	10.21	–
Calgon FCA						1.22	–	15.81	–
Calgon Sulfusorb 12						1.00	–	–	–

regard, be it on the basis of normalized or absolute COS uptake. This is perhaps surprising, and may be due to a number of confounding factors, such as the phase composition at different Ni/Mg ratios (i.e., the degree of demixing of the Ni, Mg and Al oxide phases). Additionally, the size of the mixed oxide crystallites can be expected to be influential, given that as particle size decreases the relative proportion of defect sites increases.

Of the LDH-derived mixed oxides tested, the composition with Ni/Mg/Al = 0.32/0.48/0.20 was found to show the best capacity for COS adsorption. This material also showed superior adsorption capacity to the commercial carbon-based adsorbents tested, although it was less effective than the Ag^+-exchanged zeolite (which suffers from the disadvantage that it can be expected to be significantly more expensive). Based on this promising result, the performance of this composition was tested for the adsorption of methyl mercaptan.

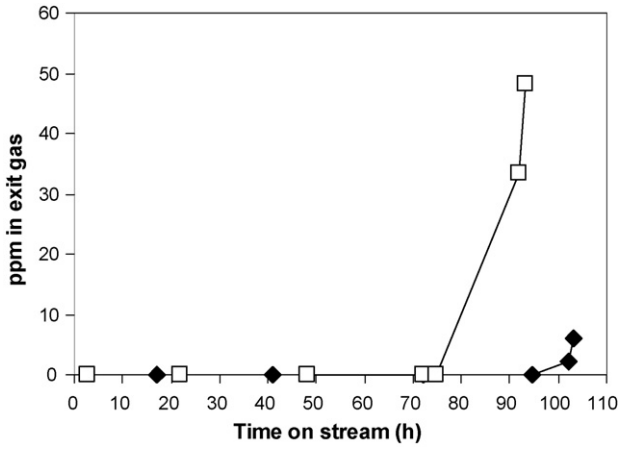

Fig. 5. Breakthrough curves for COS (◆) and CH_3SH (□) adsorption on Ni/Mg/Al = 0.32/0.48/0.20 adsorbent.

3.5. Methyl mercaptan adsorption

Adsorption experiments using CH_3SH were conducted under the same conditions as for COS adsorption, using a feed of 100 ppm CH_3SH in N_2. As for COS, in all cases the measured CH_3SH concentration at the bed outlet remained below the detection limit (~0.5 ppm) up to the breakthrough point (see Fig. 5). As shown in Table 4, the two Ni/Mg/Al mixed oxides tested (corresponding to the best two LDH-derived COS adsorbents) showed moderate adsorption capacities for CH_3SH, these being on the same order of magnitude as the capacities for COS uptake on a mole basis. In comparison, the commercial AgLiX zeolite and FCA carbon adsorbents showed significantly higher CH_3SH adsorption capacities.

3.6. Adsorbent regeneration

The ability to regenerate a spent adsorbent is an important factor if its use is to be economically attractive. Initially, attempts were made to regenerate spent Ni/Mg/Al adsorbents by heating under inert atmosphere to promote thermal desorption of the adsorbed COS. Thermogravimetric data (not shown) indicate that heating in N_2 at 450 °C results in desorption of approximately 95% of the loaded COS. However, gravimetric adsorption profiles of the treated adsorbent revealed a significant decrease in adsorption capacity. This suggests that the small amount of residual COS is able to block

Table 5
Summary of COS adsorption experiments using regenerated adsorbents

Sample	Ni	Mg	Al	Wt% COS captured			
				Fresh	After 1st regeneration	After 2nd regeneration	After 3rd regeneration
Ni/Mg/Al	0.64	0.16	0.20	1.80	2.05	1.34	1.30
Ni/Mg/Al	0.32	0.48	0.20	2.47	2.63	2.62	1.81

a significant fraction of the adsorption sites. Fixed bed adsorption/regeneration experiments confirm this picture. For example, regeneration of spent Ni/Mg/Al = 0.32/0.48/0.20 adsorbent by heating at 450 °C under N_2 for 1 h resulted in a decrease in the time required for COS breakthrough from 67 h for the fresh material, to 7 h for the regenerated material.

Regeneration was therefore attempted by heating spent adsorbent under reducing conditions (450 °C for 1 h), using a mixture of 5% H_2 in N_2. In this manner it was hoped to remove the residual sulfur species in a reduced form, e.g., as H_2S. Table 5 shows the results of fixed bed COS adsorption experiments using two different fresh and regenerated Ni/Mg/Al adsorbents. From these results it is apparent that adsorbent regeneration in the presence of H_2 is extremely effective. In all cases, the adsorbents subjected to one regeneration displayed slightly higher breakthrough capacities than in the fresh state, implying that the formation of Ni(0) is beneficial for COS adsorption. This is not surprising, given the high affinity of metallic nickel for sulfur [31,32]. Indeed, Ni nanoparticles supported on Y zeolite, alumina and mesoporous silica have recently been shown to adsorb sulfur compounds present in diesel [33–35]. Confirmation of Ni(0) formation was provided by XPS data obtained on a sample of Ni/Mg/Al = 0.32/0.48/0.20 adsorbent subjected to one adsorption/regeneration cycle. Curve fitting of the Ni $2p_{3/2}$ and $2p_{1/2}$ peaks (Fig. 6) indicates that approximately one-third of the Ni detected is present as Ni(0). The corresponding X-ray diffractogram (not shown) contained broad lines for MgO and NiO, a particle size of ~3 nm being indicated for the NiO crystallites. Metallic nickel was not detected, implying that it must be present in highly dispersed form.

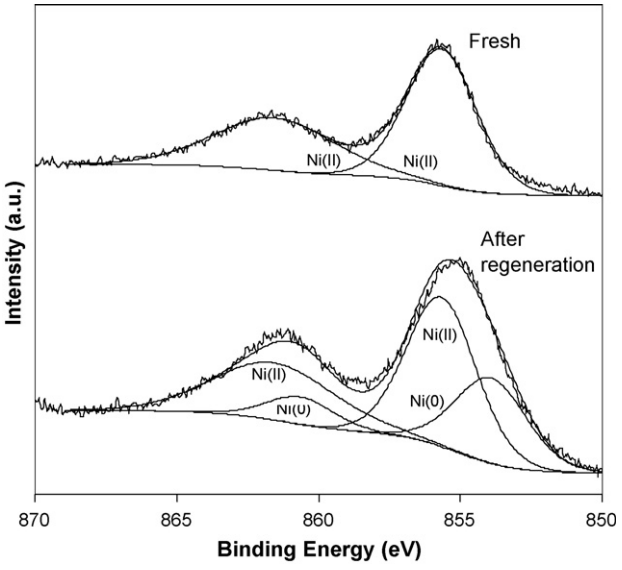

Fig. 6. XPS spectrum of Ni/Mg/Al = 0.32/0.48/0.20 adsorbent in the Ni 2p region: fresh (top) and subjected to one COS adsorption/regeneration cycle (bottom).

As shown in Table 5, repeated adsorption/regeneration cycles result in a decline in breakthrough capacity. This is most likely due either to sintering of the Ni(0) and/or Ni(II) phase, or a build up of residual sulfur. XPS analysis was therefore performed on the sample of Ni/Mg/Al = 0.32/0.48/0.20 adsorbent subjected to three cycles of adsorption and regeneration. The detection of sulfur in this sample (0.8 at.%, see Table 6) indicates that there is indeed some accumulation of sulfur due to its incomplete removal during the regeneration process. The observed binding energy of 169.0 eV is consistent with the presence of sulfate, although this may simply represent an oxidation product formed during exposure of the sample to air. XPS data are also consistent with a small degree of sintering of the Ni(0) and/or Ni(II) phase. After one cycle of adsorption/regeneration, the atomic concentrations of Ni, Mg and Al are observed to have increased relative to the uncalcined material (Table 6), due to the removal of CO_2 and H_2O during calcination. The Ni/Mg and Ni/Al ratios are noticeably decreased, however, evidencing sintering of the Ni, either during calcination or the subsequent adsorption/regeneration cycle. That the COS adsorption capacity of this material is increased relative to the fresh adsorbent (Table 5), indicates that the formation of Ni(0) more than compensates for the apparent loss in Ni dispersion with respect to overall adsorption capacity. After three adsorption/regeneration cycles the atomic concentrations of Ni and Mg are both slightly decreased relative to the material regenerated only once, while that of Al is increased, suggesting that some degree of sintering of the Ni and Mg phases occurs during repeated regenerations. This is supported by BET surface area measurements, the area of the adsorbent decreasing from 252 $m^2\,g^{-1}$ for the fresh (calcined) material to a value of 161 $m^2\,g^{-1}$ after three adsorption/regeneration cycles.

Table 6
Atomic element concentrations determined by XPS for Ni/Mg/Al = 0.32/0.48/0.20 adsorbent

Sample	Ni (at.%)	Mg (at.%)	Al (at.%)	S (at.%)	Ni/Mg	Ni/Al
Fresh[a]	8.5	8.2	7.2	0	1.04	1.18
1 × regeneration	10.6	13.4	10.8	0	0.79	0.98
3 × regeneration	9.4	11.5	14.8	0.8	0.82	0.64

[a] Uncalcined.

4. Conclusions

The results from this study indicate that LDH-derived Ni/Mg/Al mixed oxides are promising adsorbents for the removal of COS from gas streams. For Ni/Mg/Al materials with different Al contents, the materials with lower Al contents ($x = 0.20$) were found to possess higher adsorption capacities than their high Al content analogs ($x = 0.33$). This effect is not associated with the surface areas of the mixed oxides (as reflected in the normalized uptake values) and implies that the COS adsorption sites in these materials are associated with Ni^{2+} and Mg^{2+}, rather than with Al^{3+}. However, a correlation between COS adsorption capacity and the Ni/Mg ratio could not be found. Of the mixed oxides tested, the composition with Ni/Mg/Al = 0.32/0.48/0.20 showed the best capacity for COS adsorption. Treatment of the spent adsorbent under an atmosphere of 5% H_2 in N_2 at 450 °C was found to provide an effective means of restoring the adsorption capacity over two cycles of adsorption and regeneration, although after three such cycles, adsorption capacity decreased. XPS data suggested the likely cause of this decrease to be a combination of sulfur accumulation at the surface and sintering of the Ni and Mg phases.

Acknowledgements

The authors wish to thank Gerald Thomas for performing the X-ray diffraction measurements and Dr. Timothy C. Golden of Air Products and Chemicals, Inc. for providing commercial adsorbent samples. This research work was supported in part by a grant from the Kentucky Science and Engineering Foundation as per Grant Agreement #KSEF-148-502-05-134 with the Kentucky Science and Technology Corporation.

References

[1] F.A. Uribe, T.A. Zawodzinski, 2001 Joint International Meeting—The 200th Meeting of the Electrochemical Society and the 52nd Annual Meeting of the International Society for Electrochemistry, San Francisco, 2001 (abstract).
[2] P.J. de Wild, R.G. Nyqvist, F.A. de Bruijn, E.R. Stobbe, J. Power Sources 159 (2006) 995.
[3] R. Farrauto, S. Hwang, L. Shore, W. Ruettinger, J. Lampert, T. Giroux, Y. Liu, O. Ilinich, Annu. Rev. Mater. Res. 33 (2003) 1.
[4] W. Liss, W. Thrasher, G. Steinmetz, C. Howdiah, A. Attari, Am. Gas Assoc. Lab., Final Rep. GRI-29/0123, Cleveland, OH, 1992.
[5] Product information, Occidental Chemical, http://www.oxy.com/OXYCHEM/Products/odorants/odorants.htm.
[6] GPA Standard 2140-97, Gas Producers Association, Tulsa, OK.
[7] A.L. Dicks, J. Power Sources 61 (1996) 113.
[8] A. Kohl, F. Riedenfeld, Gas Purification, fourth ed., Gulf Publishing Co., Houston, 1985 (Chapter 13).
[9] C. Monereau, S. Moreau, Air Liquide, European Patent Application, 1,132,341 (2001).
[10] J.H. Taylor, J.P. Glass, G.R. Say, R.P. O'Connor, Exxon, US Patent Application, 98-12534 (1999).
[11] F. Cavani, F. Trifiró, A. Vaccari, Catal. Today 11 (1991) 173.
[12] M.A. Ulibarri, M. del Carmen, Hermosin, in: V. Rives (Ed.), Layered Double Hydroxides: Present and Future, Nova Sci. Pub. Inc., New York, 2001 (Chapter 9).
[13] D. Tichit, B. Coq, CATTECH 7 (2002) 206.
[14] B.F. Sels, D.E. de Vos, P.A. Jacobs, Catal. Rev. 43 (2001) 443.
[15] A.E. Palomares, J.M. López-Nieto, F.J. Lázaro, A. López, A. Corma, Appl. Catal. B 20 (1999) 257.
[16] Z. Yong, A.E. Rodrigues, Energy Convers. Manage. 43 (2002) 1865.
[17] T. Yamamoto, T. Kodama, N. Hasegawa, M. Tsuji, Y. Tamaura, Energy Convers. Manage. 36 (1995) 637.
[18] M. Tsuji, G. Mao, T. Yoshida, Y. Tamaura, J. Mater. Res. 8 (1993) 1137.
[19] G. Fornasari, F. Trifiro, A. Vaccari, F. Prinetto, G. Ghiotti, G. Centi, Catal. Today 75 (2002) 421.
[20] G. Centi, G. Fornasari, C. Gobbi, M. Livi, F. Trifiro, A. Vaccari, Catal. Today 73 (2002) 287.
[21] A. Corma, A.E. Palomares, F. Rey, F. Márquez, J. Catal. 170 (1997) 140.
[22] E.W. Albers, H.W. Burkhead, Jr., US Patent 5,928,496 (1999).
[23] T.J. Pinnavaia, J. Amarasekera, US Patent 5,358,701 (1994).
[24] L.T. Nemeth, S. Kulprathipanja, B.J. Arena, J.S. Holmgren, US Patent 5,360,536 (1994).
[25] W.T. Reichle, J. Catal. 94 (1985) 547.
[26] E. Chenu, G. Jacobs, A.C. Crawford, R.A. Keogh, P.M. Patterson, D.E. Sparks, B.H. Davis, Appl. Catal. B: Environ. 59 (2005) 45.
[27] S. Krumm, Winfit, available at www.xray.cz/ecm-cd/soft/xray/index0114.html.
[28] M. Tsuji, G. Mao, T. Yoshido, Y. Tamaura, J. Mater. Res. 8 (1993) 1137.
[29] J.I. Di Cosimo, V.K. Díez, M. Xu, E. Iglesia, C.R. Apesteguía, J. Catal. 178 (1998) 499.
[30] W.T. Reichle, Solid State Ionics 22 (1986) 135.
[31] E.K. Poels, W.P. van Beek, W. den Hoed, C. Visser, Fuel 74 (1995) 1800.
[32] C. Bartholomew, Stud. Surf. Sci. Catal. 37 (1987) 81.
[33] X. Ma, S. Velu, J.H. Kim, C. Song, Appl. Catal. B 56 (2005) 137.
[34] S. Velu, X. Ma, C. Song, M. Namazian, S. Sethuraman, G. Venkataraman, Energy Fuels 19 (2005) 1116.
[35] C.H. Ko, J.G. Park, J.C. Park, H. Song, S.-S. Han, J.-N. Kim, Appl. Surf. Sci. 253 (2007) 5864.